Applied Catalysis B: Environmental 156–157 (2014) 134–140

Contents lists available at ScienceDirect

Applied Catalysis B: Environmental

journal homepage: www.elsevier.com/locate/apcatb

Wedged N-doped CuO with more negative conductive band and lower overpotential for high efficiency photoelectric converting CO_2 to methanol

Peiqiang Li *, Jinfeng Xu, Hua Jing, Chenxiao Wu, Hui Peng, Jing Lu, Hongzong Yin

College of Chemistry and Material Science, Shandong Agricultural University, 271018, People's Republic of China

ARTICLE INFO

Article history:
Received 2 January 2014
Received in revised form 2 March 2014
Accepted 9 March 2014
Available online 18 March 2014

Keywords:
Wedged N-doped CuO
Photoelectrocatalytic
Carbon dioxide
Methanol
CuO film

ABSTRACT

One dimensional wedged N-doped CuO has been in situ prepared on Cu substrate by anodization method. The as-prepared material with a length of 786 nm and width of 143 nm presents uniform wedged structure. The energy band gap and conductive band is 1.34 eV and −1.03 eV, respectively. The carrier concentration of wedged N-doped CuO (7.5×10^5 m^{-3}) is about 10^8 times that of CuO film (4.8×10^{-3} m^{-3}). The as-prepared material promotes the separation of photoelectrons and holes efficiently to achieve the excellent photocatalytic reduction property. For the electrochemical properties aspect, the electrochemical adsorptive active site for CO_2 on the as-prepared material (25 nmol) is 252 times that of CuO film (99 pmol). And the overpotential shifts 0.17 V positively relative to CuO film. Furthermore, it shows outstanding electrocatalytic property for CO_2 reduction. In the process of photoelectrocatalytic reduction CO_2, the predominant product is methanol, the current efficiency on wedged N-doped CuO electrode (84.4%) is 14.5 times that of CuO film (5.84%), the methanol output (3.6 mmol L^{-1} cm^{-2}) is 139 times that of CuO film (0.026 mmol L^{-1} cm^{-2}). In addition, it shows that the methanol output in the photoelectrocatalytic process is 1.3 times of the simple addition of photocatalytic process and electrocatalytic process, which indicates the distinct 1 + 1 > 2 synergistic effect between electrocatalytic reduction and photocatalytic reduction.

1. Introduction

Global warming and resource shortage are the problems the society facing, the CO_2 emission has reached 31.6 billion metric tons on the world in 2012, which causes a series of environmental problems. As we known, CO_2 is also a very precious C1 resource, so the conversion of CO_2 to organics is not only benefit to the CO_2 emission reduction, but also contributed to the energy storage [1–3].

Photocatalytic (PC) reduction [4,5] and electrocatalytic (EC) reduction [6,7] of CO_2 have been research hotspots in recent years, because H^+ comes from water other than fossil fuel, and the reactions processes at normal temperatures and pressures, so the PC and EC methods are environmental friendly. However, there are many problems in the process of using the advanced PC or EC techniques individually. For example, low PC efficiency still exists in the PC process [8,9]. And high overpotential, large energy consumption and the des-activation of active site in EC process are the main problems we faced [10–14]. Therefore, it is particularly important to couple PC and EC in situ together to overcome the above shortcomings [15]. The former researcher paid more attention to photo-enhanced EC reduction or electric-enhanced PC reduction, but there is few research in the field of photo and electric synergistic catalytic reduction [16].

Choosing material is the key step for achieving excellent photo and electric synergistic catalytic effect. It asks for the material must own excellent PC and EC properties simultaneously. CuO is a good choice among the numerous catalysts, in the PC aspect, it can utilize visible light sufficiently for its narrow energy band gap (1.0–2.08 eV) [17], and the conductive band is located at −0.8 eV [18], the negative location of conductive band makes it possess the beautiful PC reduction ability; in the EC aspect, CuO owns good electron transfer performance and brilliant EC selectivity. Therefore, coupling PC with EC in situ to achieve synergistic photoelectrocatalytic reduction of CO_2 on CuO.

In this paper, we adopted mild anodization method to obtain one dimensional wedged N-doped CuO on Cu substrate in situ, and

* Corresponding author at: College of Chemistry and Material Science, Shandong Agricultural University, 61 Daizong Road, Tai'an, Shandong 271018, PR China. Tel.: +86 0538 8249017.
E-mail addresses: chem_carbon@outlook.com, pqli@sdau.edu.cn (P. Li).

http://dx.doi.org/10.1016/j.apcatb.2014.03.011
0926-3373/

then compared the photoelectrocatalytic (PEC) reduction of CO_2 effect with CuO film. The as-prepared wedged N-doped CuO with more negative conductive band, larger carrier concentration, bigger electrochemical absorption specific surface area and lower overpotential for CO_2 electrochemical reduction exhibits outstanding PC property as well as excellent EC property compared with CuO film. Furthermore, it embodies distinct synergistic effect between EC and PC. The research makes a guided significance on the material choosing for PEC reduction of CO_2. Meanwhile, it has important social significance on low carbon emissions our society faced.

2. Materials and methods

2.1. Preparation of catalysts

Preparation of wedged N-doped CuO: The Cu foils (20 mm × 50 mm × 1.5 mm) were firstly polished by sand papers (360 mesh) and then processed through ultrasound 5 min in absolute alcohol and dried naturally in air. The electrolytes (V_{water}:$V_{ethonal}$ = 3:1) were consisted of 3.200 g NaOH and 0.002 g polyving akohol 520. The Cu foil worked as working electrode and titanium foil worked as counter electrode. The optimization of the catalyst preparation process were listed in the supporting file (Supporting Information Figs. S1–5). The anodization experiments were performed under 3 mA cm^{-2} for 1 h (15 °C). After sonicating in ethanol and redistilled water for 10 min, respectively, and then the samples were put in a muffle furnace (KSL-1100X) under nitrogen atmosphere with the flow rate of 60 sccm (standard cubic centimeters min^{-1}) then heated to 300 °C with rate of 2 °C min^{-1} and maintained at 300 °C for 3 h. Then the samples were cooled to room temperature with the rate of 2 °C min^{-1}. Therefore, the wedged N-doped CuO was prepared.

Preparation of CuO film: The pretreatment of Cu foils followed the above method. Then Cu foils were put in the muffle furnace under oxygen atmosphere with the identical condition. Then CuO film was formed.

2.2. Characterization of catalysts

The surface morphologies of the as-prepared samples were characterized by scanning electron microscopy (SEM, Philips XL30 FEG) with accelerated voltage of 20 kV. Surface compositions were detected by X-ray photoelectron spectroscopy (XPS, ESCALAB 250) with a monochromated X-ray source (Al Kα hυ = 1486.6 eV). The UV–vis diffuse reflectance spectra (UV–vis DRS) was measured for photochemical properties using a TU-1901 in combination with a single reflection internal accessory (Beijing Purkinje General Instrument Co., Ltd.). The electrochemical properties were measured by CHI660D potentiostat (Shanghai Chen hua Instrument Co., Ltd.).

The adsorptive active site volume G calculated method was listed below: according to the Cottrell theory: $Q = n\mathrm{FG} + Q_{d1} + 2n\mathrm{FAC}^0{}_{ox}D^{1/2}t^{1/2}/\prod^{1/2}$, it can be seen from the formula that the total charge Q has a linear relationship with the $t^{1/2}$, but also the intercept in charge-axis is nFG + Q_{dl}, in the blank medium sulfate solution that the intercept is measured as Q_{dl}, the difference is nFG, thus the reaction volume G in the electrode surface can be obtained (n = 1).

2.3. Product analysis

Properties of PEC reduction of CO_2 were measured by CHI660D potentiostat with a scan rate of 50 mV s^{-1}. The as-prepared electrode, Hg/Hg_2Cl_2 in saturated KCl solution (SCE), and platinum wire worked as working electrode, reference electrode and counter electrode, respectively. CO_2 was bubbled with the flow rate of 40 sccm in 0.1 mol L^{-1} $KHCO_3$ aqueous solution for 30 min until it was saturated, then started the experiment. The electrodes were illuminated under visible light by a Xenon lamp with a band-pass filter ($\lambda \geq 420$ nm, 100 mW cm^{-2}). At the end of the electrolysis, the liquid phase was immediately sampled through the septum of the cell and analyzed by gas chromatography (GC-9A, Shimadzu). The GC was equipped with glass packed column (2 m, inner diameter 3 mm, Parapok Q, 80-100) and flame ionization detector. The column temperature was kept at 80 °C and the detector temperature was at 200 °C. High purity N_2 worked as carrier gas with a flow rate of 30 sccm. All the experimental data were conducted three times and then averaged to eradicate any discrepancies.

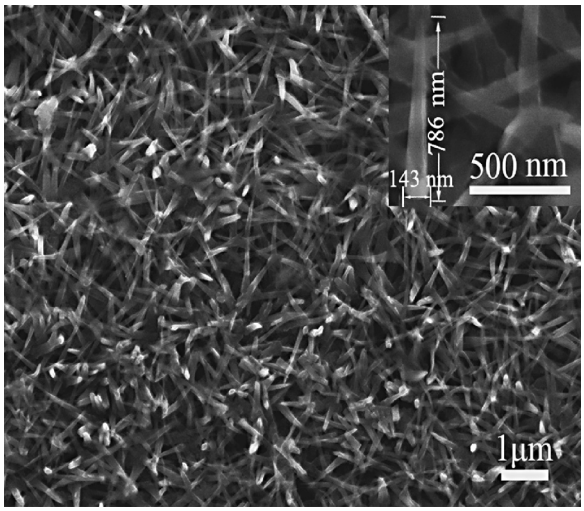

Fig. 1. SEM of wedged N-doped CuO, the insert picture is the single wedged N-doped CuO.

3. Results and discussion

From Fig. 1, it can be seen that CuO presented wedge-shaped, the wedges distributed homogenously and appeared staggered growth. The growth situation of the single wedged CuO was also can be seen clearly from the insert figure, the length and width of the single wedge is 143 nm and 786 nm, respectively, and it narrowed from the wider part to a point ultimately, which presented one dimensional wedged growth state. To the best of our knowledge, this kind of CuO structure has not been found in the literature, therefore, the one dimensional wedged CuO structure was successfully prepared for the first time.

Fig. 2a was the UV–vis DRS of wedged N-doped CuO and CuO film. CuO film presented absorption peaks at 430 nm and 550 nm, while wedged N-doped CuO emerged an apparent absorption peak at 550 nm, and the absorption was above the CuO film entirely, which appeared an obvious red shift integrally compared to CuO film. The energy band gap (E_g) was calculated by the conventional Tauc Eq. (1) below [19,20]:

$$ah\nu = A(h\nu - E_g)^{n/2} \quad (1)$$

where a, ν, A and E_g are the absorption coefficient, light frequency, proportionality constant and band gap, respectively. The E_g was calculated by a linear fit to the experimental $(\alpha h\nu)^2$ versus $h\nu$ plot (Fig. 2b). The intersection point of the tangent and horizontal ordinate is the E_g. The E_g of wedged N-doped CuO and CuO film is 1.34 eV and 1.51 eV, respectively. It indicated that the wedged N-doped CuO with narrow E_g can be irradiated easily by visible light (≤925 nm), it is consistent with the UV–vis DRS results, the band–band transition from valence band to conductive band of wedged N-doped CuO generated red shift.

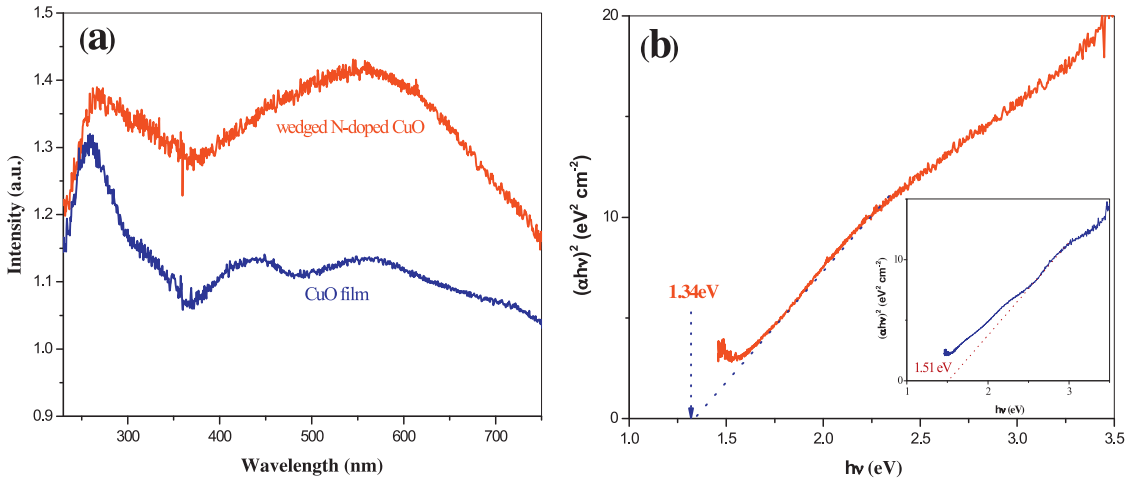

Fig. 2. (a) UV–vis DRS of wedged N-doped CuO and CuO film (b) Band gap value of wedged N-doped CuO, the insert picture is the band gap value of CuO film.

Fig. 3 described the XPS spectrum of wedged N-doped CuO, all data were adjusted based on C element. The wide scan XPS spectrum (Supporting Information Fig. S6) revealed the predominant presence of C, O, N and Cu elements. Among these elements, N, Cu, and O elements were from the as-prepared material and the C element was from the XPS instrument itself. No other hetero-elements were detected. In Fig. 3a, the two binding energy peaks located at 933.8 and 953.8 eV were assigned to Cu 2p3/2 and Cu 2p1/2 of CuO, respectively [21]. Meanwhile, there was a series of satellite peaks at around 943.8 and 962.5 eV for Cu 2p3/2 and Cu 2p1/2 in CuO, indicating the existence of an unfilled Cu 3d shell [22]. The binding energy peak locating at 399.2 eV was assigned to

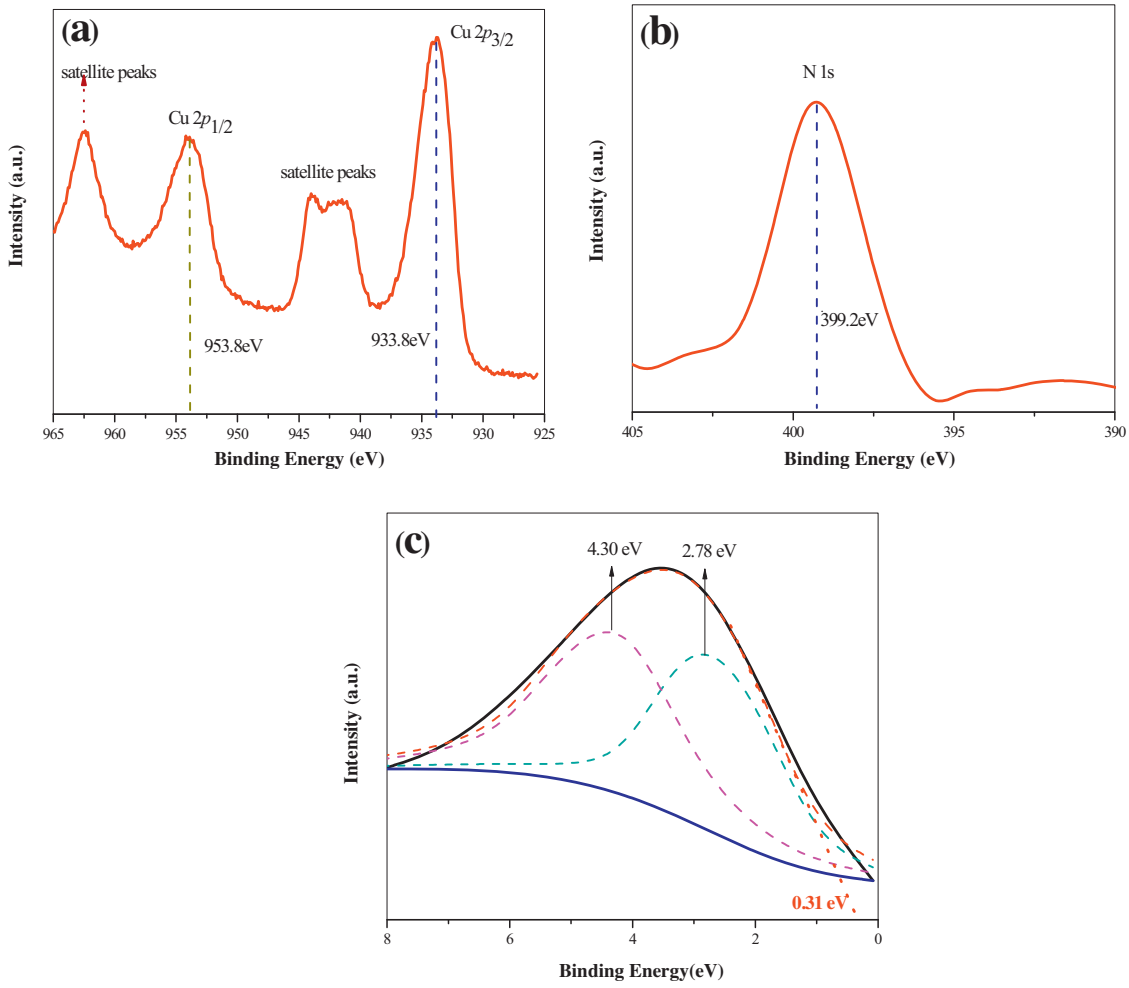

Fig. 3. (a) XPS spectrum of Cu 2p, (b) XPS spectrum of N 1s, (c) Valence band photoemission spectrum of wedged N-doped CuO (solid line) and its Gaussian fit (dashed line). The spectrum was smoothed and baseline corrected.

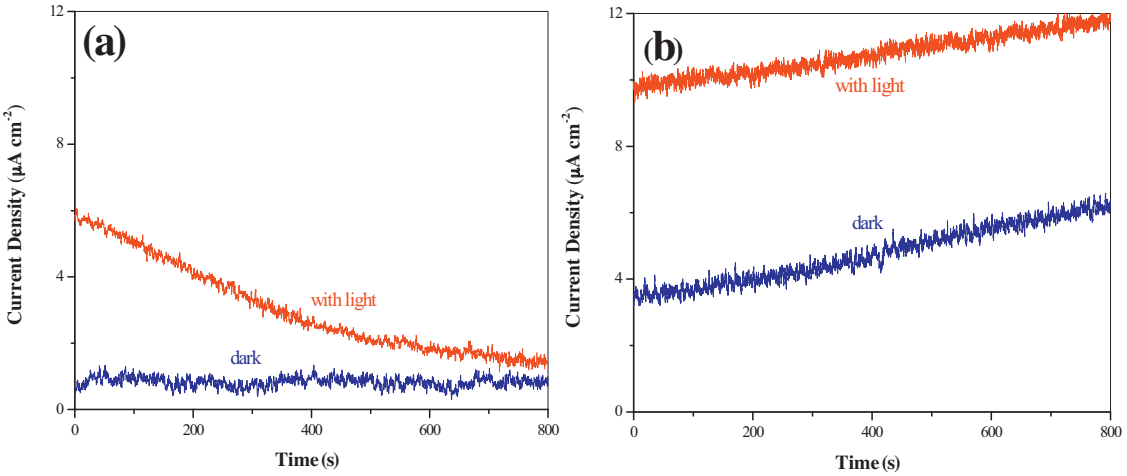

Fig. 4. *I–t* curve of CO_2 reduction under open circuit potential of (a) CuO film, (b) wedged N-doped CuO.

N 1s, it indicated the CuO was doped with N element successfully in the prepared process (Fig. 3b). In Fig. 3c, two distinguished peaks centered at 4.30 eV and 2.78 eV were shown in the photoemission spectrum, which attributed to the p (nonbonding) and s (bonding) electron emissions from O2p orbitals, respectively. The location of the valence band maximum (VBM) was determined directly from the electron emission spectrum by method of a linear extrapolation of the onset of the valence band emission [23]. The VBM was found to be 0.31 eV, and it generated negative shift compared to literature [18]. Therefore, electron in the valence band is easier to be irradiated to the conductive band, thus the electron and hole could separate very well. Meanwhile, the negative shift of the valence band is beneficial to lower the applied voltage for CO_2 reduction, so the lower applied voltage could drive the CO_2 reduction reaction [24]. It could be further obtained that the conductive band minimum (CBM) locating at −1.03 eV according the energy band gap of 1.34 eV (Fig. 2b). The CBM of wedged N-doped CuO shifted negatively compared with CBM of CuO in the literature (−0.8 eV).

The light responses of the electrodes for CO_2 reduction under open circuit potential in the CO_2-saturated 0.1 mol L^{-1} $KHCO_3$ aqueous solution were shown in Fig. 4. I_{light} and I_{dark} presents the current density with light and without light, respectively. Light sensitivity ($I_{SE} = I_{light} - I_{dark}$) was used to show the current density difference value for CO_2 reduction with light and without light. Initially, CuO film (I_{SE1}) was about 5.11 μA cm^{-2}, wedged N-doped CuO (I_{SE2}) was about 6.20 μA cm^{-2}, I_{SE2} was 1.2 times as many as I_{SE1}; after 800 s, I_{SE2} (5.61 μA cm^{-2}) was 9.6 times as many as I_{SE1} (0.58 μA cm^{-2}). The experiment data above indicated that the I_{SE1} of CuO film declined obviously, however, the wedged N-doped CuO (I_{SE2}) was almost invariable. It was presumed that the one dimensional structure and N-doping were beneficial to the separation of photoelectrons and holes, which promoted the photo-generated charge carrier density, and then revealed outstanding PC properties and light stability.

In order to study the PC properties of wedged N-doped CuO further, the Mott-Schottky curves were explored. When the charge carrier density of oxidation film space charge region presented exhausted state through the applied potential adjustment, the space charge region capacity (C_{sc}) and the applied potential (E) would conform with the Mott-Schottky Eq. (2) below [25]:

$$\frac{1}{C_{SC}^2} = -\frac{2}{\varepsilon_0 \varepsilon_r N_A A^2}\left(E - E_{FB} - \frac{kT}{e}\right) \quad (2)$$

where C_{sc}, ε_0, ε_r, N_A, A, E, E_{FB}, k, T and e are the space charge region capacity, permittivity of vacuum (8.854×10^{-12} F m^{-1}), passive film relative dielectric constant under room temperature (CuO is 25) [26], acceptor concentration, the contact area between the electrode and solution (4 cm^2), applied potential, flat band potential, Boltzmann constant (1.38×10^{-23} J K^{-1}), thermodynamic temperature (K) and electronic charge (1.602×10^{-19} C), respectively, at room temperature, kTe^{-1} is about 25 mV could be ignored in general (Fig. 5).

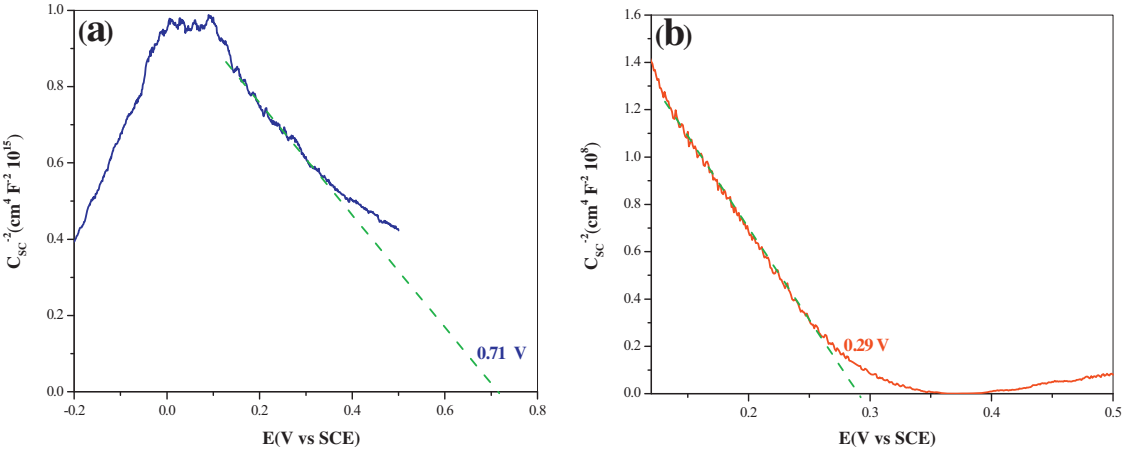

Fig. 5. Mott-Schottky plot of (a) CuO film, (b) wedged N-doped CuO.

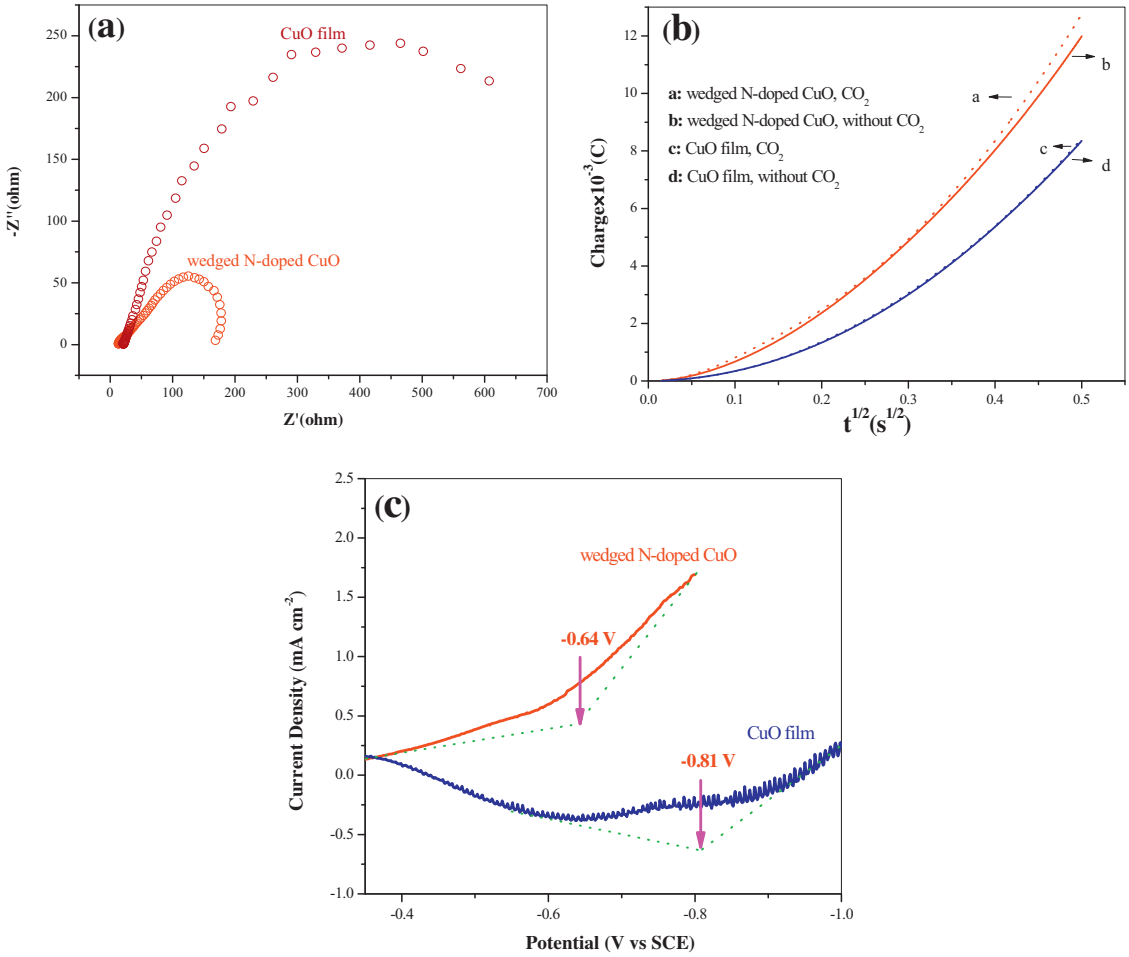

Fig. 6. (a) EIS of wedged N-doped CuO and CuO film, (b) chronocoulometry curves on wedged N-doped CuO and CuO film, (c) EC reduction of CO_2 on wedged N-doped CuO and CuO film.

The Mott-Schottky plot was obtained by the experimental Csc^{-2} versus E. Constructing the tangent line of the longest linear part, the negative slope indicated CuO film and wedged N-doped CuO both are p-type semiconductors, which were in agreement with literatures. The point of the tangent line and the horizontal ordinate is E_{FB}, which is 0.71 V and 0.29 V. The VBM of p-type semiconductor is located at 0.1–0.2 V below the flatband potential [27], thus the VBM of wedged N-doped CuO is located at 0.39–0.49 V approximately, which is in accordance with VBM value obtained from XPS spectrum. Taking E_{FB} into the Mott-Schottky equation, the acceptor concentration N_A could be obtained (4.8×10^{-3} m^{-3} and 7.5×10^{5} m^{-3}), it can be seen obviously that the wedged N-doped CuO is 10^8 times as many as CuO film, this result demonstrated that one dimensional wedged N-doped CuO was better for the separation of photoelectrons and holes. At the same time, N element in wedged N-doped CuO could not change the semiconductor type of CuO, but the new shallow acceptor band provided by N 2p orbit contributed to the carrier mobility irradiated by light [28,29], it is the reason why the PC activity of wedged N-doped CuO is higher than CuO film. Electrons from the valence band is easy to be irradiated to the intermediate band preferentially, and then further to the conductive band, so the addition of intermediate band is conducive to broaden the absorbing wavelength range, which is easier to be irradiated by visible light. However, CuO film without shallow acceptor band is difficult to be irradiated by visible light compared with wedged N-doped CuO. Consequently, wedged N-doped CuO exhibits more excellent PC properties and light stability, which is in keeping with Fig. 4.

Fig. 6a is the Electrochemical Impedance Spectroscopy (EIS) of wedged N-doped CuO and CuO film, it can be seen clearly that the EIS of wedged N-doped CuO (175 Ω) was smaller than that of CuO film (650 Ω), which demonstrated one dimensional wedged N-doped CuO structure was more beneficial for the electron transmission. In order to obtain the electrochemical adsorption surface area, the chronocoulometry curves were conducted on wedged N-doped CuO and CuO film in Fig. 6b. Curves b and a were the chronocoulometry curves on wedged N-doped CuO with and without CO_2, curves d and c were the chronocoulometry curves on CuO film with and without CO_2. The adsorptive active site on wedged N-doped CuO was 25 nmol, which is 252 times that of CuO film (99 pmol). It demonstrated that wedged N-doped CuO with larger electrochemical adsorption surface area could be able to provide more electrochemical reaction active site to the subsequent CO_2 reduction.

Fig. 6c was obtained by the following method: Firstly, N_2 was purged into $KHCO_3$ with the rate of 40 sccm for 30 min, and then conducted linear sweep voltammetry (LSV); after that, CO_2 was plunged for 30 min until it was saturated, then repeated the experiment. The CO_2 reduction and hydrogen evolution reaction (HER) are competitive reactions on the surface of the electrode, so saturated N_2 electrolyte was used to take off HER. Fig. 6c was obtained by taking off background, which reflected the EC reduction of CO_2

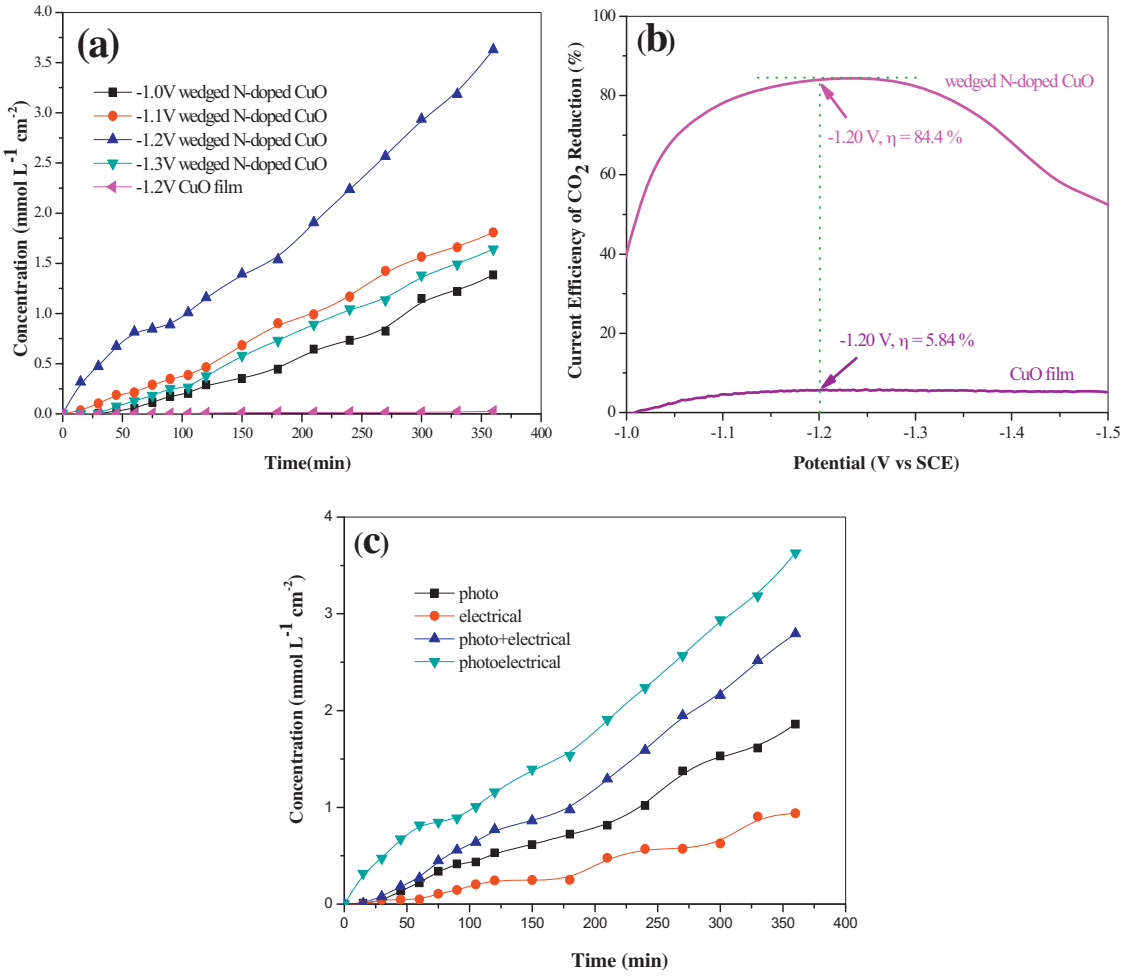

Fig. 7. (a) PEC reduction of CO_2 on wedged N-doped CuO and CuO film under different potentials, (b) current efficiency of PEC reduction of CO_2 on wedged N-doped CuO and CuO film, (c) PEC, PC and EC reduction of CO_2 on wedged N-doped CuO.

property on wedged N-doped CuO sufficiently. As known from the Fig. 6c, the onset potential for CO_2 EC reduction on wedged N-doped CuO and CuO film was −0.64 V and −0.81 V, which illustrated it could be realized CO_2 EC reduction with smaller applied potential on wedged N-doped CuO, so wedged N-doped CuO showed better EC properties. This result is consistent with the literatures that it needs relatively smaller applied potential to EC reduction of CO_2 efficiently when the VBM location shifts negatively [24].

Ultimately, the products analysis of PEC reduction of CO_2 were conducted, the predominant product was methanol confirmed by GC. Fig. 7a was the product for PEC reduction of CO_2 varied with time under different applied potentials on wedged N-doped CuO, methanol output increased initially and then decreased with the applied potential from −1.0 V to −1.3 V, and it reached a maximum (3.6 mmol L^{-1} cm^{-2}) under −1.2 V after 6 h, it was only 0.026 mmol L^{-1} cm^{-2} on CuO film at this moment. Methanol output on wedged N-doped CuO was 139 times as many as CuO film, which demonstrated wedged N-doped CuO exhibits more outstanding PEC property for the reduction of CO_2. In addition, the almost invariable methanol product rate could illustrate that the wedged N-doped CuO possesses excellent stability.

For the existence of methanol maximum for PEC reduction of CO_2, we interpreted it from the current efficiency. The current efficiency η was calculated as followed (3):

$$\eta = \frac{J_a - J_b}{J_a} \times 100\% \quad (3)$$

J_a is the current density with continious bubbling CO_2, J_b is the current density with continious bubbling N_2. Because the CO_2 reduction and HER are competitive reactions on the surface of the electrode. $J_a - J_b$ can be almost reflected the net current density of CO_2 reduction. Thus corresponding efficiency (η) of PEC CO_2 reduction could be calculated.

The current efficiency for PEC reduction of CO_2 varied with different applied potential on wedged N-doped CuO and CuO film was shown in Fig. 7b, the current efficiency on CuO film electrode increased to 5.84% and then maintained with the negative shift of applied potential; while it existed a maximum (84.4%) on wedged N-doped CuO electrode under −1.2 V was 14.5 times that of CuO film. Therefore, one dimensional wedged N-doped CuO exhibits more excellent PEC property for the reduction of CO_2, it is an inevitability for the material with more negative conduction band potential, larger carrier concentration, more electrochemical active site and lower applied potential properties.

At the same time, the photoelectric synergistic effect was further explored on the wedged N-doped CuO in Fig. 7c. The applied potential −1.2 V showing the largest current efficiency for CO_2 reduction was choosed to conduct the experiment. After 6 h, the methanol output of EC, PC, simple addition of EC and PC, and PEC was 0.94 mmol L^{-1} cm^{-2}, 1.80 mmol L^{-1} cm^{-2}, 2.74 mmol L^{-1} cm^{-2}, 3.60 mmol L^{-1} cm^{-2}, respectively. We found that the methanol output was 1.3 times of the simple addition, what indicated it produced distinct 1 + 1>2 synergistic effect between EC and PC.

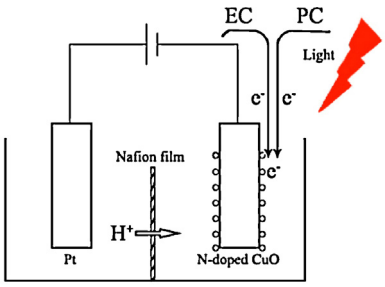

Scheme 1. The mechanism of PEC reduction of CO_2.

The possible mechanism of PEC process of the wedged N-doped CuO showed as Scheme 1. The formation of CH_3OH from CO_2 mechanism equation is:

$$CO_2 + 6e^- + 6H^+ = CH_3OH + H_2O$$

Protons are produced from the oxidation of water on anode, they pass through the proton exchange membrance to reach the cathode surface to participate in the reaction. In the process of PEC, one hand, the catalyst with conduction band (−1.03 eV) is irradiated by light to produce high reducing ability electrons; on the other hand, the extra applied voltage could provide electrons continuously to join the reduction of CO_2, the two aspects result in the PEC synergistic effect.

4. Conclusions

In conclusion, one dimensional wedged N-doped CuO has been in situ prepared on Cu substrate by anodization method firstly. The as-preparede N-doped CuO with a length of 786 nm and width 143 nm presents wedged structure uniformly. The energy band gap and conductive band is 1.34 eV and −1.03 eV, respectively. The carrier concentration of wedged N-doped CuO (7.5×10^5 m^{-3}) is about 10^8 times that of CuO film (4.8×10^{-3} m^{-3}). The as-prepared material not only exhibites excellent PC reduction property, but also promotes separation of photoelectrons and holes efficiently. For the electrochemical properties aspect, the electrochemical adsorptive active site for CO_2 on the as-prepared material (25 nmol) is 252 times that of CuO film (99 pmol). And the overpotential shifts 0.17 V positively relative to CuO film. Furthermore, it shows outstanding EC property for CO_2 reduction. In the process of PEC reduction CO_2, the predominant product is methanol, the current efficiency on wedged N-doped CuO electrode (84.4%) is 14.5 times of CuO film (5.84%), the methanol output (3.6 mmol L^{-1} cm^{-2}) is 139 times of CuO film (0.026 mmol L^{-1} cm^{-2}). Furthermore, it shows that the methanol output in the PEC process was 1.3 times of the simple addition of PC process and EC process, which indicated the existence of distinct 1 + 1>2 synergistic effect between PC reduction and EC reduction.This study has significance on CO_2 emission reduction and CO_2 cyclic utilization for C1 resource, meanwhile, it has a certain guidance and reference significance on PEC synergistic reduction of CO_2.

Acknowledgements

This research was supported by the National Natural Science Foundation of China (Grant No. 21203114), Key Projects in the National Science & Technology Pillar Program during the Twelfth Five-year Plan Period (Grant No. 2011BAD11B01), and Promotive Research Fund for Excellent Young and Middle-aged Scientists of Shandong Province (Grant No. BS2012NJ008), and Science and Technology Development Planning of Shandong province (Grant No. 2013GZX20109). We are grateful to the foundation supported by Shandong Jingbo Holdings Corporation.

Appendix A. Supplementary data

Supplementary material related to this article can be found, in the online version, at http://dx.doi.org/10.1016/j.apcatb.2014.03.011.

References

[1] P. Richardson, M.L. Perdigoto, W. Wang, R.J. Lopes, Appl. Catal. B: Environ. 132 (2012) 408–415.
[2] Q. Liu, Y. Zhou, J. Kou, X. Chen, Z. Tian, J. Gao, S. Yan, Z. Zou, J. Am. Chem. Soc. 132 (2010) 14385–14387.
[3] E.E. Barton, D.M. Rampulla, A.B. Bocarsly, J. Am. Chem. Soc. 130 (2008) 6342–6344.
[4] S.I. In, D.D. Vaughn, R.E. Schaak, Angew. Chem. Int. Ed. 51 (2012) 3915–3918.
[5] S. Qin, F. Xin, Y. Liu, X. Yin, W. Ma, J. Colloid Interface Sci. 356 (2011) 257–261.
[6] A. Mao, K. Shin, J.K. Kim, D.H. Wang, G.Y. Han, J.H. Park, ACS Appl. Mater. Interfaces 3 (2011) 1852–1858.
[7] C.W. Li, M.W. Kanan, J. Am. Chem. Soc. 134 (2012) 7231–7234.
[8] J. Yu, J. Ran, Energy Environ. Sci. 4 (2011) 1364–1371.
[9] S. Navalón, A. Dhakshinamoorthy, M. Álvaro, H. Garcia, ChemSusChem 6 (2013) 562–577.
[10] N.S. Spinner, J.A. Vega, W.E. Mustain, Catal. Sci. Technol. 2 (2012) 19–28.
[11] E.E. Benson, C.P. Kubiak, A.J. Sathrum, J.M. Smieja, Chem. Soc. Rev. 38 (2009) 89–99.
[12] M. Le, M. Ren, Z. Zhang, P.T. Sprunger, R.L. Kurtz, J.C. Flake, J. Electrochem. Soc. 158 (2011) E45–E49.
[13] A.J. Morris, R.T. McGibbon, A.B. Bocarsly, ChemSusChem 4 (2011) 191–196.
[14] Y. Chen, C.W. Li, M.W. Kanan, J. Am. Chem. Soc. 134 (2012) 19969–19972.
[15] J. Yuan, C. Hao, Solar Energy Mater. Solar Cells 108 (2013) 170–174.
[16] B. Kumar, M. Llorente, J. Froehlich, T. Dang, A. Sathrum, C.P. Kubiak, Ann. Rev. Phys. Chem. 63 (2012) 541–569.
[17] M. Lai, S. Mubeen, N. Chartuprayoon, A. Mulchandani, M.A. Deshusses, N.V. Myung, Nanotechnology 21 (2010) 295601.
[18] S.C. Roy, O.K. Varghese, M. Paulose, C.A. Grimes, ACS Nano 4 (2010) 1259–1278.
[19] Y. Wang, Y.-n. Zhang, G. Zhao, H. Tian, H. Shi, T. Zhou, ACS Appl. Mater. Interfaces 4 (2012) 3965–3972.
[20] K. Nakaoka, J. Ueyama, K. Ogura, J. Electrochem. Soc. 151 (2004) C661–C665.
[21] Y. Sakai, S. Ninomiya, K. Hiraoka, Surf. Interface Anal. 44 (2012) 938–941.
[22] P. Wang, Y.H. Ng, R. Amal, Nanoscale 5 (2013) 2952–2958.
[23] L. Larina, O. Shevaleevskiy, B.T. Ahn, Energy Environ. Sci. 4 (2011) 1480–1486.
[24] R. Asahi, T. Morikawa, T. Ohwaki, K. Aoki, Y. Taga, Science 293 (2001) 269–271.
[25] K. Gelderman, L. Lee, S. Donne, J. Chem. Educ. 84 (2007) 685.
[26] S. Sarkar, P.K. Jana, B. Chaudhuri, H. Sakata, Appl. Phys. Lett. 89 (2006) 212905–1212905.
[27] C.G. Read, Y. Park, K.-S. Choi, J. Phys. Chem. Lett. 3 (2012) 1872–1876.
[28] S. Matsushima, K. Obata, H. Nakamura, M. Arai, K. Kobayashi, J. Phys. Chem. Solids 64 (2003) 2417–2421.
[29] S. Kim, S.-J. Hwang, W. Choi, J. Phys. Chem. B 109 (2005) 24260–24267.